15

Experimental π Phase-Shifts Observed in the Fourier Spectra of Phase Gratings and Applications in Simultaneous PSI

Noel-Ivan Toto-Arellano[1], Gustavo Rodríguez-Zurita[2], Amalia Martínez-García[1], David-Ignacio Serrano-García[1] and María-Graciela Hernández-Orduña[3]
[1]*Centro de Investigaciones en Óptica A.C. León, Gto.,*
[2]*Benemérita Universidad Autónoma de Puebla,*
[3]*Instituto Tecnológico Superior de Misanta, Ver.*
México

1. Introduction

Through the use of a great variety of interferometric techniques, simultaneous phase shifting interferometry can be implemented to study dynamic events. Most of these techniques use expensive components; therefore, it is convenient to develop simultaneous phase shifting techniques that employ more accessible elements.

Recent studies show that a grating can be used as a beam splitter to attain several interference patterns around each diffraction order. Since each pattern has to show a different phase-shift, a suitable shifting technique must be employed, and phase gratings are attractive to perform the former task due to their higher diffraction efficiencies.

As it is very well known, the Fourier coefficients of only-phase gratings are integer order Bessel functions of the first kind. The values of these real-valued functions oscillate around zero, so they can adopt negative values, thereby introducing phase shifts of π at certain diffraction orders. Because of this, an almost trivial fact seems to have been overlooked in the literature regarding its practical implications.

In this chapter such phase shifts are presented in the description of interference patterns obtained with grating interferometers. These patterns are obtained by means of a two beam interferometer using a Mach Zehnder arrangement. The beams interfere at the object plane of a 4-*f* system with a sinusoidal grating/grid on the Fourier plane. It is shown the corresponding experimental observations of the fringe modulation, as well as the corresponding phase measurements, are all in agreement with the proposed description. A simultaneous phase shifting interferometer is finally proposed taking into account these properties after proper incorporation of polarization modulation.

2. Basic considerations

Phase gratings have been employed as an optical element with more efficiency than absorption gratings to perform a variety of tasks. Among them are beam splitting for interferometry, intensity measuring (Azzam, 1982) and optical shop testing (Ronchi, 1964; Cornejo, 1992). Their performance strongly depends upon their Fourier spectra, and for the case of sinusoidal phase grating has been extensively discussed (Barrekette and Freitag, 1963) It is well known that their Fourier coefficients are Bessel functions of the first kind of integer order q, J_q (Goodman, 1988) ; such functions are real valued, and their values oscillate around zero, so they can eventually introduce π-phase shifts into a given grating Fourier spectrum. These shifts were of little relevance, if any, to applications where power spectrum is the main concern, as is often the case in spectroscopy (Kneubühl, 1969) , but recently, it has been pointed out that a grating interferometer with two windows on the object plane performs a common path interferometer (Arrizón and Sánchez, 2004). Several advantages have been shown about this interferometers, i.e. their mechanical stability (Meneses et al., 2006). Moreover, in conjunction with a suitable modulation of polarization, single-shot phase-shifting interferometric systems can be implemented with phase gratings (Rodriguez et al., 2008). Two-beam phase-grating interferometers (TBPGI) are based on the interference between neighboring diffraction orders. Thus, the fringe modulation of each interference pattern can be affected when π-phase shifts are present (Rodriguez, 2008; Thomas, 1976). Furthermore, these phase shifts have to be taken into account for the overall performance of the system, and their practical advantages can even influence its design. This chapter is first aimed at the phase shifts between diffraction orders that have been observed in the Fourier spectra of a phase grating. An example of phase sinusoidal grating is calculated with a standard FFT routine that is useful for the interpretation of later experimental observations.

Experimental observations in agreement with the previous discussions, are shown by using commercial phase gratings, and finally, as an application of the above, a system able to obtain n-interferograms captured in one shot.

2.1 Experimental setup

The optical system proposed is shown in Fig. 1. Basically, it consists of a combination of a quarter-wave plate Q and a linear polarizing filter P_0 that generates linearly polarized light oriented at a $45°$ angle entering the Mach Zehnder configuration from a YVO_3 laser operating at 532 nm (see Fig. 1). This configuration generates two symmetrically displaced beams by moving mirrors M and M', enabling one to change the spacing x_0 between beam centers. Two retardation plates (Q_L and Q_R) with mutually orthogonal fast axes are placed in front of the two beams (A, B) to generate left and right nearly-circular polarized light (Novak et al., 2005; Rodrigurez 2008). A phase-grating $G(u/\lambda f, v/\lambda f)$ is placed on the frequency plane (u,v) of the 4-f Fourier optical system that is coupled to the Mach Zehnder configuration, with f being the focal length of each transforming lens. Then, $\mu = u/\lambda f$ and $\upsilon = v/\lambda f$ are the frequency coordinates scaled to the wavelength λ and the focal length. On plane (μ,υ), the period of G is denoted by d, and its spatial frequency by $\sigma = 1/d$. Two neighboring diffraction orders have a distance of $F_0 \equiv \lambda f / d$ at the image plane for a grating; then, $\sigma \cdot u = F_0 \cdot \mu$ and F_0 can be used as a frequency. In the following sections, phase shifts at the image plane of this system due to the grating are discussed.

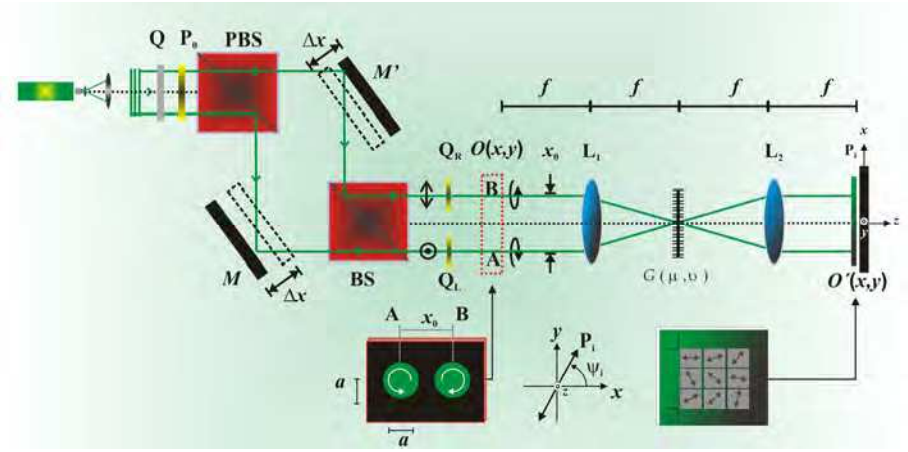

Fig. 1. Experimental setup for the Two Beam Phase Grating Interferometer using a phase grating $G(\mu,\upsilon)$ of period d placed in a 4-*f* system at the end of a Mach Zehnder configuration.

3. Sinusoidal phase gratings

For simplicity, we will consider a sinusoidal phase grating centered on the Fourier plane of a 4-*f* system. Its complex amplitude can be expressed as

$$G(\mu,\upsilon)=e^{i2\pi\cdot A_g\sin[2\pi F_0\mu]}=\sum_{q=-\infty}^{\infty}J_q\left(2\pi A_g\right)e^{i2\pi\cdot qF_0\mu} \tag{1}$$

with $2\pi A_g$ being the grating's phase amplitude and J_q the Bessel function of the first kind of integer order q. The Fourier transform of Eq. 1 is then given by

$$\tilde{G}(x,y)=\sum_{q=-\infty}^{\infty}J_q\left(2\pi A_g\right)\delta(x-qF_0,y) \tag{2}$$

with $\delta(x,y)$ as the two-dimensional Dirac delta function. Thus, the Fourier spectrum of a sinusoidal phase grating comprises point-like diffraction orders of amplitude weighted by Bessel functions. Such spectrum can be detected at the image plane of the 4-*f* system.

3.1 Phase grids

A sinusoidal phase grid can be generated through the multiplication of two sinusoidal phase gratings whose respective grating vectors are forming a 90-degree angle. Taking the rulings of one grating along the "μ" direction and the rulings of the second grating along the "υ" direction, the resulting centered phase grid can be written as

$$G_2(\mu,\upsilon) = e^{i2\pi A_g \sin[2\pi\cdot X_0\mu]}\, e^{i2\pi A_g \sin[2\pi\cdot Y_0\upsilon]} = \sum_{q=-\infty}^{\infty} J_q\left(2\pi A_g\right) e^{i2\pi\cdot qF_0\mu} \sum_{r=-\infty}^{\infty} J_r\left(2\pi A_g\right) e^{i2\pi\cdot rF_0\upsilon} \quad (3)$$

where the frequencies along each axis direction are taken as $X_0 = Y_0 = F_0$. The Fourier transform of the phase grid becomes

$$\tilde{G}_2(x,y) = \sum_{q=-\infty}^{q=\infty} \sum_{r=-\infty}^{r=\infty} J_q\left(2\pi A_g\right) J_r\left(2\pi A_g\right) \delta\left(x - qF_0, y - rF_0\right), \quad (4)$$

which also consists of point-like diffraction orders distributed on the image plane on the nodes of a lattice with a period given by value F_0.

4. Two-windows phase-grating interferometry: interference-pattern contrasts and modulation

Phase grating interferometry is based on a phase grid placed as the pupil of a 4-*f* Fourier optical system. The use of two windows at the object plane, in conjunction with phase grating interferometry, allows interference between the optical fields associated to each window with higher diffraction efficiency (Arrizón, 2004 and Meneses, 2006); such system performs as a common path interferometer (Fig. 1). A convenient pair of windows for a grating interferometer implies an amplitude transmittance given by

$$O(x,y) = w(x + \frac{x_0}{2}, y) + w'(x - \frac{x_0}{2}, y) \quad (5)$$

where x_0 is the separation from center to center between two beams. For simplicity, considering a rectangular aperture $w(x,y)$, written as $w(x,y) = rect[x/a]\cdot rect[y/b]$ and $w'(x,y) = w(x,y)\exp\{i\phi(x,y)\}$, with $\phi(x,y)$ as the object phase function. As shown in Fig. 2, a and b represent the side lengths of each beam (A and B). Placing a grating of spatial period $d = \lambda f / F_0$ at the Fourier plane, with a corresponding transmittance given by $G(\mu,\upsilon)$. The image formed by the system consists basically of replications of each window at distances F_0. This image is defined by $O'(x,y)$; that is, the convolution of $O(x,y)$ with the Fourier transform of the phase grating, $\tilde{G}(x,y)$ represented by

$$\begin{aligned} O'(x,y) &= O(x,y) * \tilde{G}(x,y) \\ &= w\left(x + \frac{x_0}{2}, y\right) * \sum_{q=-\infty}^{\infty} J_q(2\pi A_g)\,\delta\left(x - qF_0, y\right) \\ &+ \left[w\left(x - \frac{x_0}{2}, y\right) e^{i\phi\left(x - \frac{x_0}{2}, y\right)} \right] * \sum_{q=-\infty}^{\infty} J_q(2\pi A_g)\,\delta\left(x - qF_0, y\right). \end{aligned} \quad (6)$$

where (*) denotes the convolution. By adding the terms of Eq. 6, taking q and q-1 (both located within the same replicated window $w\left(x - qF_0 + \frac{x_0}{2}, y\right)$), and for the case of matching

the beams' positions with the diffraction order's positions ($F_0 = x_0$), the previous equation simplifies to

$$O'(x,y) = \sum_{q=-\infty}^{\infty} \left[J_q(2\pi A_g) + J_{q-1}(2\pi A_g) e^{i\phi\left(x - x_0\left[q-\frac{1}{2}\right], y\right)} \right] w\left(x - x_0\left[q-\frac{1}{2}\right], y\right) \tag{7}$$

Thus, an interference pattern between fields associated to each window must appear within each replicated window. The fringe modulation m_q of each pattern would be of the form

$$m_q = \frac{2J_q J_{q-1}}{J_q^2 + J_{q-1}^2} \tag{8}$$

Further phase-shifting techniques must be used in order to introduce proper additional shifts into each pattern. One possible technique to be used is through an appropriate displacement of the grating (Meneses 2006), and an alternative approach is the use of the polarization-induced phase shifting (Rodriguez 2008a) method used and the one depicted in Fig. 1.

4.1 π–shifts of the Fourier spectra of sinusoidal phase gratings

According to Eq. 8, m_q and the contrast of each interference pattern depend on the signs of J_q and J_{q-1}; thus, the signs of J_q are also relevant. For the case of $\phi(x,y) = 0$, this relationship is shown on Table 1 for some cases of q. For q = 0,-1,-2,-3,-4 , a negative contrast is expected; otherwise, it would be positive.

$q = 0$	$J_0 + J_{-1} = J_0 - J_1$	$q = -1$	$J_{-1} + J_{-2} = -J_1 + J_2$
$q = 1$	$J_1 + J_0$	$q = -2$	$J_{-2} + J_{-3} = J_2 - J_3$
$q = 2$	$J_2 + J_1$	$q = -3$	$J_{-3} + J_{-4} = -J_3 + J_4$
$q = 3$	$J_3 + J_2$	$q = -4$	$J_{-4} + J_{-5} = J_4 - J_5$

Table 1. Bessel coeficients. Sign relations of superimposed orders. Case $\phi(x,y) = 0$.

Interference fringe modulation is positive for one half of the diffraction orders if the grating's Fourier coefficients are all positive for $q > 0$, whereas the other half would show alternating fringe modulation due to the odd parity of J_{2q+1}. These results can also be depicted as in Fig. 2 for a hypothetical case, where only the signs of the amplitudes of the diffraction orders from a given grating are separately shown displaced from the origin due to the respective displacement of windows A and B (first two plots from above). The case of $J_4 < 0$ is shown.

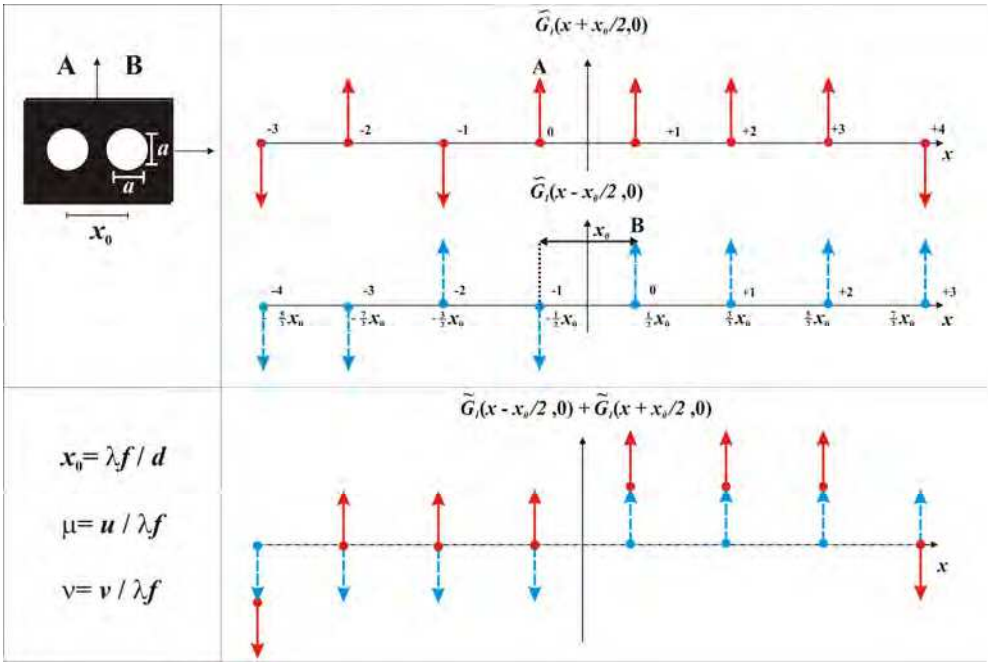

Fig. 2. Amplitude signs of diffraction orders (hypothetical grating) on the image plane of a TBPGI resulting from a window displacement of $\pm x_0 / 2$. Upper left: window configuration.

For simplicity, the replicated windows are not plotted. The third row on the graph exhibits the superposition of the two previous spectra. Fringe modulation changes must appear in both halves of the image plane. In this case, the expected signs of each fringe modulation would be +,-,-,-,+,+,+,- from left to right. The Fig. 2 then shows that odd diffraction orders have odd-order Bessel function parity, and conversely for even diffraction orders and even parity. Figure 3 shows a case of positive J_q values for q = 0,1,4,5, and negative for q = 2, 3, 6 as an example (left). This situation corresponds to the value of $2\pi A_g = 26.5$, which belongs to a range in the Bessel domain within the 9th lobule of J_0. A phase grating of the type represented by Eq. 1 (with the same amplitude $2\pi A_g$ as before) has a Fourier spectrum whose components show π–shifts accordingly (see the positive orders on the right of Fig. 3). π-shifts such as these can be detected as changes in the signs of fringe modulations in the experimental interferometers discussed later.

4.2 Some examples of calculated Fourier spectra: sinusoidal phase gratings.

In order to show some cases of phase-shifts in grating spectra, several fast Fourier transforms have been calculated for gratings of different phase amplitudes A_g. We use the lobules of J_0 as a reference to indicate the Bessel region within which the amplitude A_g of the corresponding phase grating is to be found. Only seven Bessel functions are shown in Fig. 4. In the first case, within the first lobule of J_0, the associated spectrum results with one half of

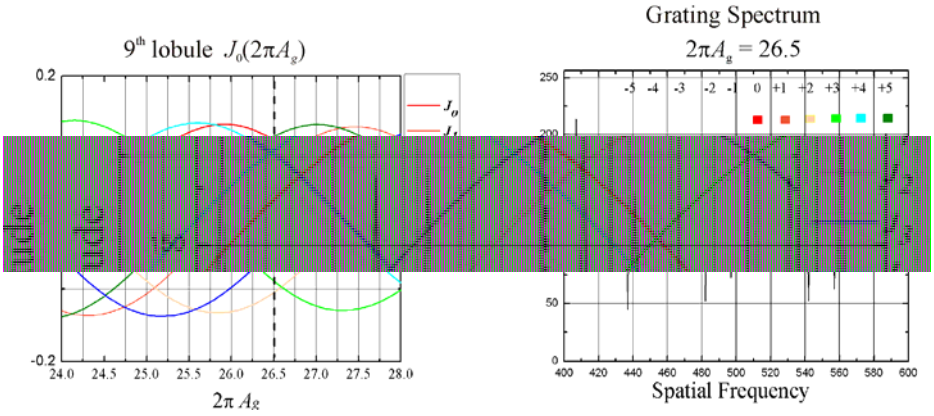

Fig. 3. Bessel domain for the ninth lobule of J_0 (left). Corresponding Fourier spectrum of the phase grating (right).

its Fourier components in phase, while the other half shows phase shifts of π in an alternating fashion. In this region, J_0 is positive and in phase with the Fourier components of the first half above mentioned. For the second case, J_0 is negative. Taking a value of A_g such that the Bessel functions with q = 1…6 take only positive values, the Fourier spectrum of the resulting grating turns out to be similar to the first case, with J_0 being negative as the only different phase shift. Within the 3th lobule, it is possible to pick up negative values for q = 1, 2, 3, with the resulting Fourier spectrum showing π-shifts accordingly. In Fig.4 , a case of positive values for q = 1,2,3 and negative for q = 4,5 is shown. This situation corresponds to a region within the 9th lobule of J_0.

4.3 π–shifts of the Fourier spectra of sinusoidal phase grids

A rectangular phase grid $G(\mu,\upsilon)$ can be generated with two phase gratings of equal spatial frequency. Fig. 5(a) depicts the signs of the diffraction orders of a grid made up from two crossed gratings having spectra as those of the one in Fig. 2. Positive signs are denoted by hollow circles, whereas negative signs are marked with crosses. The dashed lines form regions enclosing diffraction orders of index pairs 0,n or m,0. Then, order 0,0 is found at the intersection of these regions. Two possible window configurations can be considered for a TBPGI; these configurations are shown in Fig. 5(b), and they are denoted by $\mathbf{W}_1$ and $\mathbf{W}_2$. The respective displacements of the diffraction patterns are indicated with displaced dashed lines too. For the case of phase grids with windows in configuration $\mathbf{W}_2$, the image can be written as:

$$\begin{aligned} O'(x,y) &= O(x,y) * \tilde{G}_2(x,y) \\ &= \sum_{q=-\infty}^{\infty} w\left(x+\frac{x_0}{2}, y+\frac{x_0}{2}\right) * J_q(2\pi A_g) J_r(2\pi A_g)\,\delta(x-qF_0, y-rF_0) \\ &+ \sum_{q=-\infty}^{\infty} w'\left(x-\frac{x_0}{2}, y-\frac{x_0}{2}\right) * J_q(2\pi A_g) J_r(2\pi A_g)\,\delta(x-qF_0, y-rF_0). \end{aligned} \tag{9}$$

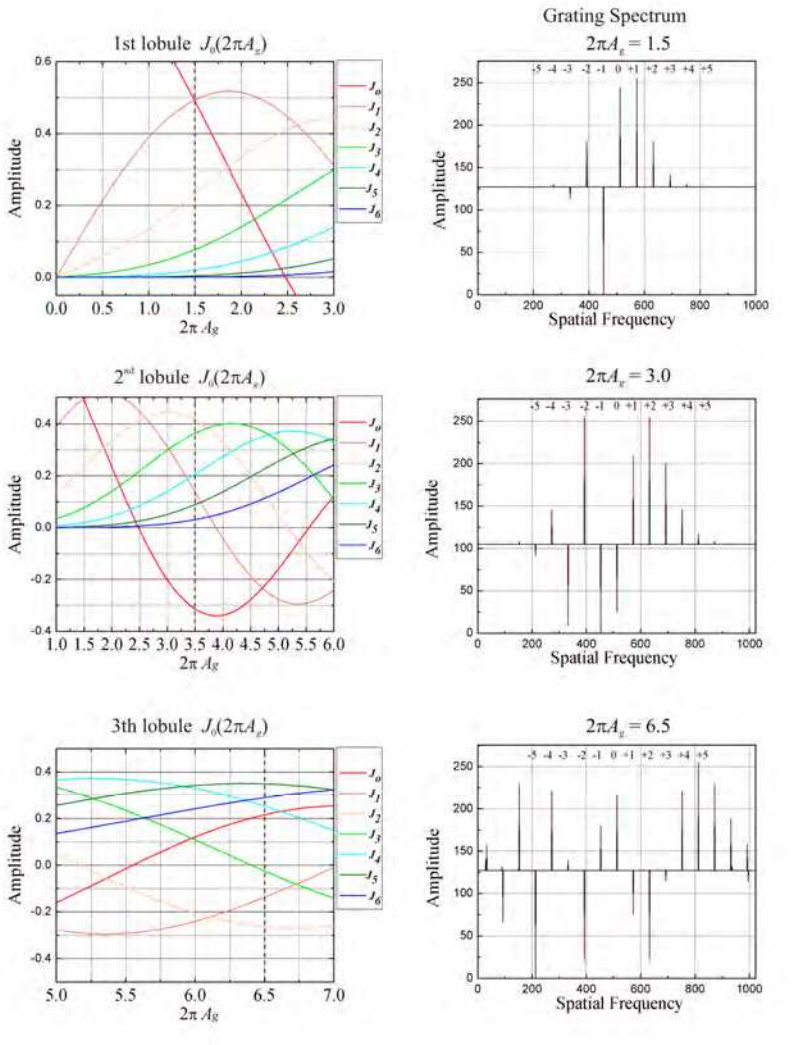

Fig. 4. Fourier spectra of phase gratings: left column, Bessel region (first seven Bessel functions shown); right column, grating spectra.

Again, with $F_0 = x_0$

$$O'(x,y) = \sum_{q=-\infty}^{\infty}\sum_{r=-\infty}^{\infty} J_q(2\pi A_g) J_r(2\pi A_g)\, w\left(x + \frac{x_0}{2}[1-2q], y + \frac{x_0}{2}[1-2r]\right) + \sum_{q=-\infty}^{\infty}\sum_{r=-\infty}^{\infty} J_{q-1}(2\pi A_g) J_{r-1}(2\pi A_g)\, w'\left(x - \frac{x_0}{2}[1-2q], y - \frac{x_0}{2}[1-2r]\right), \quad (10)$$

where $O(x,y) = w\left(x+\frac{x_0}{2}, y+\frac{x_0}{2}\right) + w\left(x-\frac{x_0}{2}, y-\frac{x_0}{2}\right)$. This result simplifies to

$$O'(x,y) = \sum_{q=-\infty}^{\infty}\sum_{r=-\infty}^{\infty}\left[J_q(2\pi A_g)J_r(2\pi A_g) + J_{q-1}(2\pi A_g)J_{r-1}(2\pi A_g)e^{i\phi\left\{\left(x-x_0\left[q-\frac{1}{2}\right]\right),\left(y-x_0\left[r-\frac{1}{2}\right]\right)\right\}}\right] \times w\left(x-x_0\left[q-\frac{1}{2}\right], y-x_0\left[r-\frac{1}{2}\right]\right). \quad (11)$$

As it is for gratings, fringe modulation of the interference pattern within a window centered in $\left(x_0\left[q-\frac{1}{2}\right], x_0\left[r-\frac{1}{2}\right]\right)$ is

$$m_{qr} = \frac{2J_qJ_{q-1}J_rJ_{r-1}}{(J_qJ_r)^2 + (J_{q-1}J_{r-1})^2} \quad (12)$$

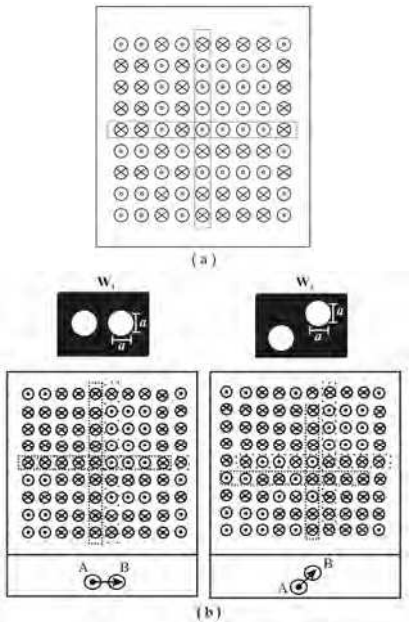

Fig. 5. (a) π-phase distribution of diffraction orders of grids. Dashed lines enclose diffraction orders of indexes 0,*n* or *m*,0. b) TBPGI order superposition: Configuration $\mathbf{W}_1$: interference pattern signs for windows displaced along the horizontal axis. Configuration $\mathbf{W}_2$: interference patterns signs for displaced windows along a line at 45°. Respective displacements of diffraction patterns are highlighted by dashed lines. An explanation of dot and cross patterns is to be found in the text.

Each corresponding fringe modulation depends on the relative phases between J_q, J_{q-1}, J_r and J_{r-1}. These relationships are discussed with the same example of Fig. 5(a). Fig. 5(b) shows the relative phases (and thus, expected signs of m_{qr}) of each diffraction order arising from configuration $\mathbf{W}_1$ or $\mathbf{W}_2$. If positive signs or negative ones coincide in a diffraction order, fringe modulation will be positive, and this is plotted with one symbol (cross or hollow dot). Only when a cross with a hollow dot appears, modulation is expected to be negative. "Vertical" bands whose sign is equal to that of m_{qr} are thus expected in configuration $\mathbf{W}_1$. Regions with a sign that is equal to that of m_{qr} can be seen in configuration $\mathbf{W}_2$.

4.4 Phase shifting interferometry with modulation of polarization

Turning the attention to gratings, in order to introduce additional phase shifts in the interference pattern centered at $(x_0[q-(1/2)], y)$ for 4-step phase-shifting (Schwieder et al., 1983), each of the windows is illuminated with different polarizations using retarding plates Q_R and Q_L (Fig. 1). This arrangement introduces Jones polarization vectors $\vec{J}_R$ and $\vec{J}_L$ into the interference terms of Eq. 6 through appropriate modification of Eq. 5. After placing a linear polarizing filter with the transmission axis at an angle ψ, its irradiance results as being proportional to

$$\left\|\vec{J}_T\right\|^2 = A(\xi,\alpha')\left\{\left({J_q}^2 + {J_{q-1}}^2\right) + 2J_qJ_{q-1}\cos[\xi(\psi,\alpha') - \phi(x,y)]\right\} \tag{13}$$

Where ψ is the linear polarizer angle, $\pm\alpha'$ the retardation of each plate, and $\xi(\psi,\alpha')$ denotes the phase shifting term induced by modulation of polarization given by

$$\xi(\psi,\alpha') = ArcTan\left[\frac{\sin[2\psi]\cdot\sin[\alpha'] + \sin^2[\psi]\cdot\sin[2\alpha']}{\cos^2[\psi] + \sin^2[\psi]\cdot\cos[2\alpha'] + \sin[2\psi]\cdot\cos[\alpha']}\right], \tag{14}$$

and $A(\psi,\alpha')$ is defined as

$$A(\psi,\alpha') = 1 + \sin[2\psi]\cos[\alpha']. \tag{15}$$

For phase-shifting interferometry with four patterns, four irradiances can be used, each one taken at a different ψ angle. Denoting each pattern as

$$\left\|\vec{J}_i\right\|^2 = A(\xi,\alpha')\left\{\left({J_q}^2 + {J_{q-1}}^2\right) + 2J_qJ_{q-1}\cos[\xi(\psi_i,\alpha') - \phi(x,y)]\right\} \tag{16}$$

with i = 1…4, the relative phase can be calculated as (J. Schwieder 1983)

$$\tan\phi = \frac{\left\|\vec{J}_1\right\|^2 - \left\|\vec{J}_3\right\|^2}{\left\|\vec{J}_2\right\|^2 - \left\|\vec{J}_4\right\|^2}, \tag{17}$$

where $\left\|\vec{J}_1\right\|^2$, $\left\|\vec{J}_2\right\|^2$, $\left\|\vec{J}_3\right\|^2$ and $\left\|\vec{J}_4\right\|^2$ are the intensity measurements with the values of ψ such that $\xi(\psi_1)=0, \xi(\psi_2)=\pi/2, \xi(\psi_3)=\pi, \xi(\psi_4)=3\pi/2$, respectively. Note that $\xi(\psi,\pi/2)=2\psi$ and $A(\psi,\pi/2)=1$, so a good choice for the retarders is quarter-wave retarders, as it is well known. Dependence of ϕ on the coordinates of the centered point has been simplified to *x,y*. The same fringe modulation m_q results as in Eq. 8. Therefore, the discussion about fringe modulation given in previous sections is retained when introducing the modulation of polarization. Such polarization modulation can also be made for grids, resulting in similar conclusions.

5. Experimental testing of the phase-shifts in phase gratings and phase grids

Figure 6 shows the superposition of Fourier amplitude spectra under window configuration $\boldsymbol{W}_1$ for a phase grating with 110 lines/mm. The contrast of the corresponding experimental interference patterns can be interpreted as if its first four Fourier coefficients had phase relations as the ones sketched in Fig. 2. They were obtained with the system of Fig.1 before placing the retardation plates Q_R, Q_L and the polarizing filters on the image plane. The patterns show the relative phases of the diffraction orders discussed in previous sections. The phase-shifted steps of the experimental fringe patterns can be calculated by applying the algorithm proposed by Kreis, 1986. The resulting mean values are shown in Table 2. It can be seen from the table that they depart by small amounts from π or 0.

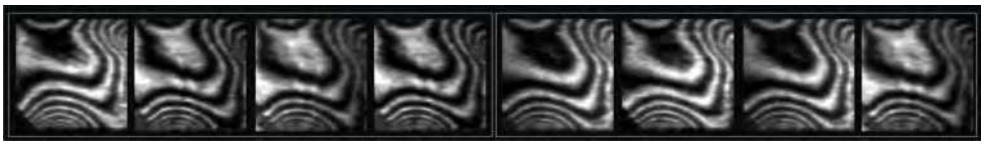

Fig. 6. Experimental results with a phase-grating.

g_1	g_2	g_3	g_4	g_5	g_6	g_7	g_8
0.00	3.143	3.130	3.150	0.010	0.014	0.003	3.145

Table 2. Phase shifts measured from experimental patterns in Fig.6 according to the method from Kreis, 1986.

Due to that, the interference patterns are obtained from the interference between the replicas of each beam, centered around each diffraction order. Fig. 7(a) presents the replicas of window A with right circular polarization, and the replicas of window B with left circular polarization; each order is superposed depending on separation x_0. Fig. 7(b) presents the interference pattern generated by the interference of windows AB, due to the cross circular polarization, a linear polarizer is placed to modulate the phase shift on each replicated interference pattern.

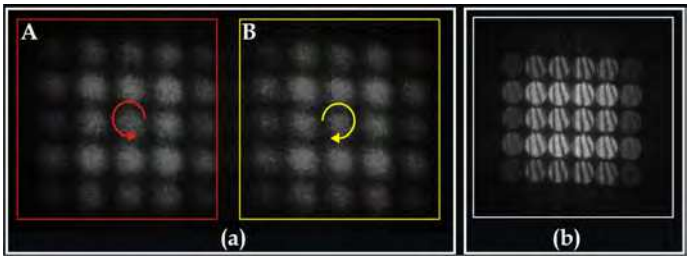

Fig. 7. Replicated windows generated by the Phase grating. (a) Replicas of A and B. (b) Interference pattern obtained through order diffraction superposition. (window configuration $\mathbf{W}_1$).

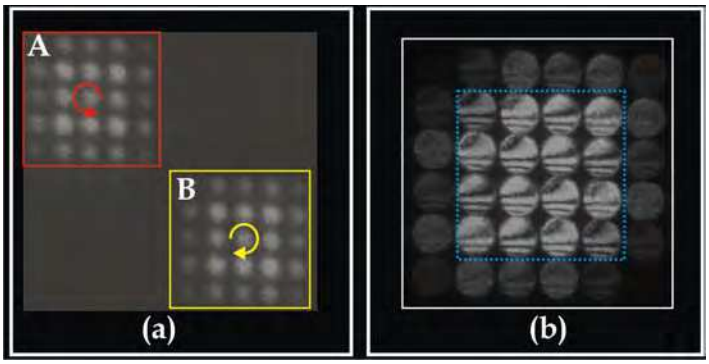

Fig. 8. Replicated windows generated by the Phase grating. (a) Replicas of A and B. (b) Interference pattern obtained through order diffraction superposition. (window configuration $\mathbf{W}_2$).

For the case of the diffraction orders belonging to a phase-grid constructed with two crossed gratings of equal frequency, the corresponding interference patterns are shown in Fig.8 for window configuration $\mathbf{W}_2$. Each grating gives patterns as in Fig. 6 when placed alone in the system of Fig. 1, with neither plate retarders nor polarizers. In each case, contrasts are in agreement with the conclusions derived from Fig. 5(b). The relative phase values of the 16 patterns within the square drawn in the patterns of Fig. 8(b) employing the method from Kreis, 1986 can be seen in Table 3.

g_1	g_2	g_3	g_4
0.010	0.030	3.120	3.152
0.016	0.020	3.140	3.141
3.145	3.150	3.136	0.020
3.139	3.170	3.182	0.043

Table 3. Phase shifts measured by means of the Kreis method for $\mathbf{W}_2$ configuration presented in Fig. 8.

6. Phase-grid interference patterns with modulation of polarization

Incorporating modulation of polarization, a TBPGI can be used for dynamic interferometry measurements. This system is able to obtain n-interferograms phase-shifted with a single shot. Phase evolving in time can be calculated and displayed on the basis of phase-shifting techniques with four or more interferograms. The system performs as previous proposals to attain four interferograms with a simultaneos capture (Barrientos et al., 1999; Novak et al., 2005). The system uses a grid as a beam splitter in a way that resembles the well-known double-frequency shearing interferometer as proposed by Wyant 1986, but our proposal differs from it not only due to its modulation of polarization, the use of a single frequency and the use of two windows, but also in the phase steps that our system introduces. Besides, our system is not a shearing interferometer of any type.

Figure 1 shows the arrangement of a simultaneous phase-shifting grid interferometer including modulation of polarization with retarders for the beams and linear polarizers on the image plane. The system generates several diffraction orders of similar irradiances, but not of equal fringe modulations, as expected (Eq. 12). In order to use Eq. 17 properly, each interferogram image was scaled to the same values of grey levels (from 0 to 255) and normalized. In the previous section, it was shown that a simplification for the polarizing filter array can be attained when using the π–phase shifts obtain values of ξ of 0, π/2, π and 3π/2. For configuration $\mathbf{W_2}$ (Fig. 8), due to the π-shifts, only two linear polarizing filters have to be placed (instead of four filters, as when without the π-shifts). The transmission axes of filter pairs P_1, P_3 and P_2, P_4 can be the same for each as long as they cover two patterns that are 180° phase apart (Fig. 9). Considering the polarizers angles , according with Sec. 4.3, the needed values of ψ can be $\psi_1 = 0°$ and $\psi_2 = 46.577°$ (G Rodriguez 2008a). They are sketched in Fig. 9. The square enclosing the 16 window replicas in the same figure is to be compared with the similar square of Fig. 8(b) (dotted lines).

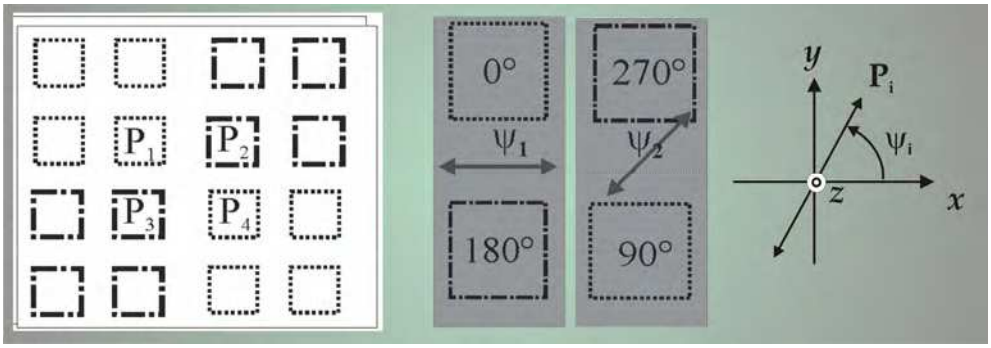

Fig. 9. Polarizing filters array for 90° phase stepping.

7. Simultaneous phase shifting interferometry

In order to extract phase distributions that evolve in time using phase-shifting interferometry, simultaneous capture of several interferograms with a prescribed shift has to be done. The well-known four-step phase shifting algorithm is presented. Due to the

capability of TBPGI to capture more than four interferograms in a single shot by placing a phase grid, we have the advantage of analyzing the case of more than four interferograms; the case of $n=(N+1)$ interferograms has been chosen. This method reduces errors in phase calculations when noisy interferograms are involved (Malacara and Servin, 2005). It the next sections of the chapter, we will show experimental results for $n = 9$ interferograms.

7.1 Four interferogram case

A phase dot was placed in the path of beam B, while beam A was used as a reference; the results obtained are shown in Fig. 10. Fig. 10(a) shows the four patterns with $\pi/2$ phase shifts obtained in a single shot, and Fig. 10(b) presents the phase profile of the object, in false color coding. However, more than four interferograms could be used, whether for *N*-steps phase-shifting interferometry (Rodriguez, 2008b) or for averaging images with the same shift.

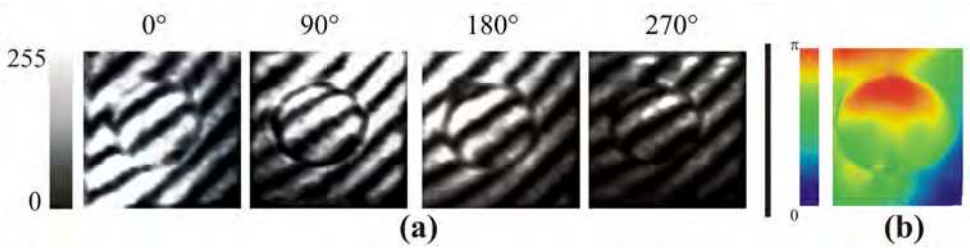

Fig. 10. Static test objects: Phase dot. (a) Four 90° phase-shifted interferograms. (b) Unwrapped phase.

Figure 11 shows the case of moving distributions, corresponding to water flowing on a microscope slide; it shows the phase profile resulting of phase evolution $\phi(x,y,t)$. Fig. 12, by analyzing flow motion by gravity, shows the temporal evolution of oil flow, clearly showing the phase changes induced by the motion of oil; the evolution of the drops as they go by in front of the camera can be shown. Images are presented in 4-D (Wyant 2003).

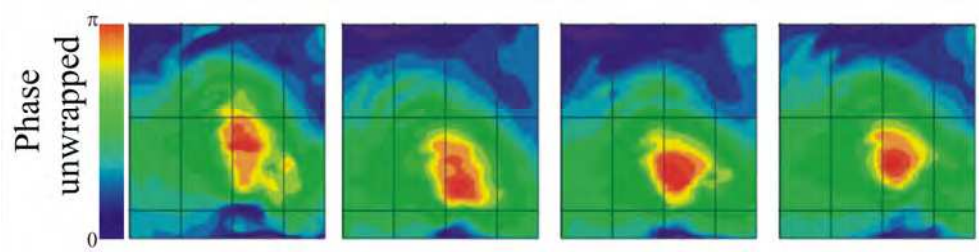

Fig. 11. Moving distributions. Representative Frames. Evolution of the phase, one capture per second.

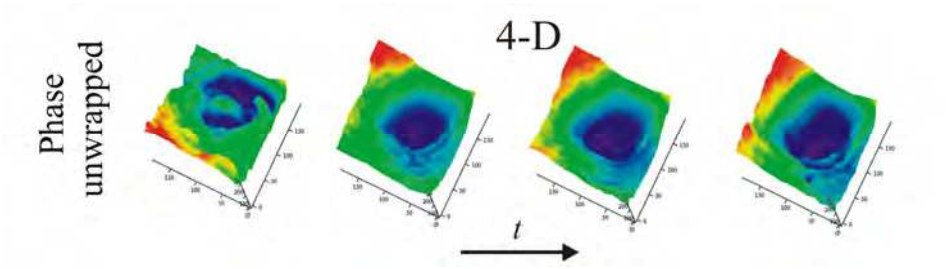

Fig. 12. Moving distributions. Oil drops moving under gravity on a slide. One capture per second.

7.2 Case of nine interferograms

To demonstrate the use of several interferograms, we choose the symmetrical n=*N*+1 phase steps algorithms, for data processing (case *N*=8). A constant phase shift value of $2\pi/N$ is employed when using these techniques. The phase shifts of p due to the grid spectra allow the use of a number of polarizing filters that is less than the number of interferograms, simplifying the filter array (See Fig. 13).

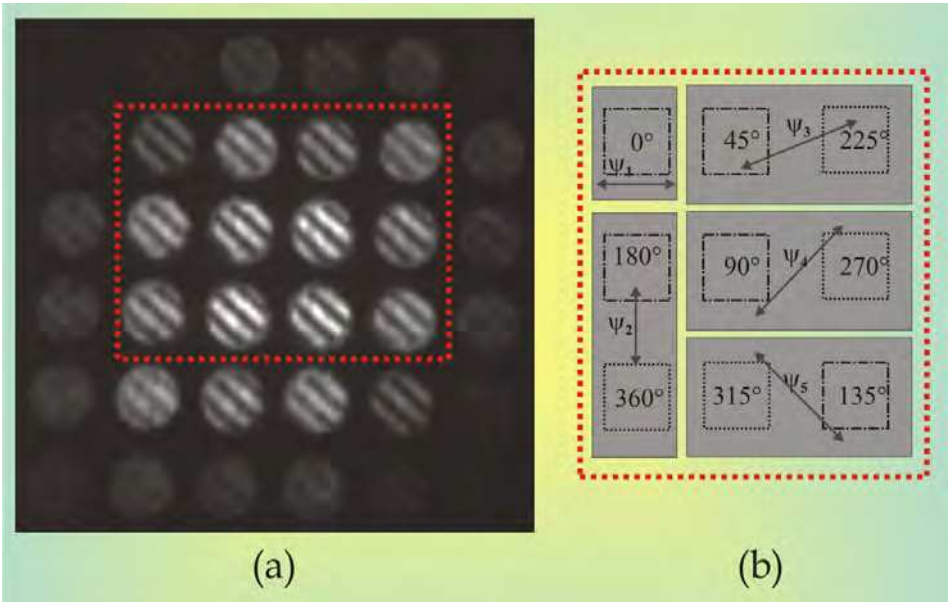

Fig. 13. Interference patterns detected with a polarizing filter at $\psi = 25°$. (a)The interference patterns used are enclosed in the dotted rectangle. (b) Polarizer filter array for N= 8, nine symmetrical interferograms.

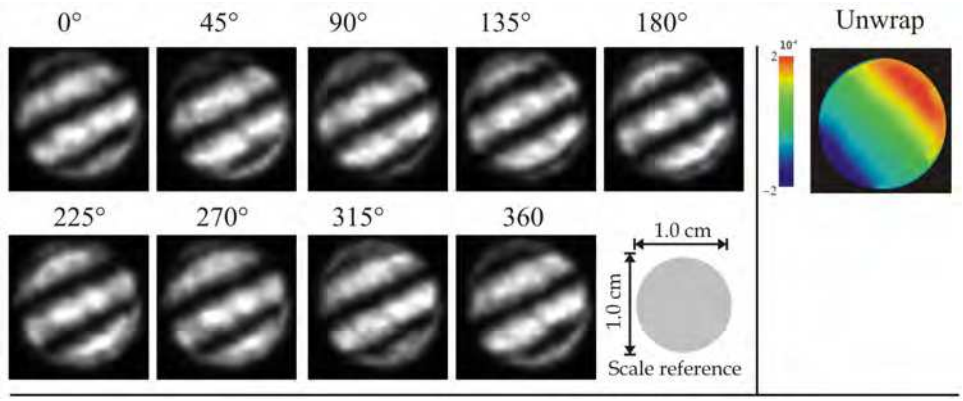

Fig. 14. Tilted wave-front. (a) Nine 45° phase-shifted interferograms (b) Unwrapped phase data map.

Considering the retarders at disposal, according to Rodriguez 2008b, it can be shown that for symmetrical nine, $\psi_1 = 0°$, $\psi_2 = 92.989°$, $\psi_3 = 22.975°$, $\psi_4 = 46.577°$ and $\psi_5 = 157.903°$. In this case, each resulting step ξ corresponds to a 45° phase-shift. The corresponding results and calculated phases are shown in Fig. 14, the experimental results shows the interference pattern generated by a tilted wavefront. That is said before, this systems are capable of obtaining $n = N+1$ interferograms in a single capture (this case, $n \leq 12$).

8. Final remark

Theoretical and experimental evidence of π–shifts in the Fourier spectra of phase gratings and phase grids were presented; these shifts are not discussed in the literature as far as we know. When the power spectrum is focused, it tends to hide the effect presented, but it can be of considerable relevance when gratings or grids are used for interferometric applications. For example: in phase shift interferometry, these results are convenient since only one grating displacement is necessary to capture four interferograms, and for the case of polarization phase shifting interferometry, the characteristics of the phase gratings used simplify the placement of polarization filters and allow us to obtain *n*-patterns in one shot.

As a final remark the system presented does not use a physical double window; it generates two beams with variable separation according to the characteristics of the grid used. The combination of circular polarization states and the use of phase-grid enable the generation of *n*-interference patterns with independent phase shifts. This characteristic optimizes the interferometric system used, and allows the analysis of static and dynamic phase distributions.

9. Acknowledgments

Authors thank M. A. Ruiz for his contribution in proofreading the manuscript. Partial support from "Consejo Nacional de Ciencia y Tecnología (CONACYT)" and "Centro de

Investigaciones en Óptica A.C. (CIO)" through projects 290597 (CONACYT-CIO) and 124145 (CONACYT-BUAP) is also acknowledged. Author *NITA* expresses sincere appreciation to *Luisa*, M*iguel* and *Damian-El* for the support provided, and to CONACYT for grant 102137/43055. Author DISG (Grant:227470/31458) is very grateful to CONACyT for the graduate scholarship granted and expresses sincere appreciation to *Geliztle*.

10. References

Arrizón V. and Sánchez-De-La-Llave D., (2004). Common-Path Interferometry with One-Dimensional Periodic Filters, *Opt. Lett.* Vol. 29, pp. 141-143.

Azzam R. M. A., (1982). Division-of-Amplitude Photopolarimeter (DOAP) for the Simultaneous Measurement of all Four Stokes Parameters of Light, *Opt. Acta,* Vol. 29, pp. 685-689.

Barrekette E. S., Freitag H., (1963). Diffraction by a Finite Sinusoidal Phase Grating, *IBM Journal*, pp. 345-349.

Barrientos-García B., Moore A. J., Pérez-López C., Wang L., and Tschudi T.,(1999) Spatial Phase-Stepped Interferometry using a Holographic Optical Element, *Opt. Eng*. Vol. 38, pp. 2069-2074.

Cornejo-Rodríguez A. (1992). Ronchi Test, in *Optical Shop Testing*.

Goodman, Jooseph W.; J. Wiley & Sons (1988). *Introduction to Fourier optics.*

Kneubühl F.,(1969). Diffraction Grating Spectroscopy, *Appl. Opt.*, Vol. 8, pp. 505-519.

Kreis T., (1986). Digital Holographic Interference-Phase Measurement Using the Fourier-Transform Method, *J. Opt. Soc. Am. A,* Vol. 3, pp. 847-855.

Malacara D., Servin M., and Malacara Z.; Marcel Dekker (1998). *Interferogram Analysis for Optical Testing*.

Meneses-Fabian C., Rodriguez-Zurita G., and Arrizon V. (2006). Common-Path Phase-Shifting Interferometer with Binary Grating, *Opt. Commun.* Vol. 264, pp. 13-17.

Novak M., Millerd J., Brock N., North-Morris M., Hayes J. and Wyant J.C., (2005). Analysis of a micropolarizer array-based simultaneous phase-shifting interferometer, *Appl. Opt.*, Vol. 44, pp. 6861-6868.

Rodriguez-Zurita G., Meneses-Fabian C., Toto-Arellano N., Vázquez-Castillo J. F. and Robledo-Sánchez C., (2008). One-Shot Phase-Shifting Phase-Grating Interferometry with Modulation of Polarization: case of four interferograms," *Opt. Express*, Vol. 16, 7806-7817.

Rodriguez-Zurita G., Toto-Arellano N. I., Meneses-Fabian C. and Vázquez-Castillo J. F., (2008). One-shot phase-shifting interferometryfive, seven, and nine interferograms, *Opt Letters*, Vol. 33, pp. 2788- 2790.

Ronchi V.,(1964). Forty Years of History of a Grating Interferometer, *Appl. Opt.*, Vol. 3, pp. 437-451.

Schwieder J., Burow R., Elssner K.-E., Grzanna J., Spolaczyk R. and Merkel K., (1983). Digital Wave-Front Measuring Interferometry: some systematic error sources, *Appl. Opt.*, Vol. 22, pp. 3421-3432.

Thomas D. A. and Wyant J. C., (1976). High Efficiency Grating Lateral Shear Interferometer, *Opt. Eng.*, Vol. 15, pp. 477.

Wyant J. C., (1973). Double Frequency Grating Lateral Shear Interferometer, *Appl. Opt.*, Vol. 12, pp. 2057-2060.
Wyant J. C., (2003). Dynamic Interferometry, *Optics & Photonics News*, Vol. 14, pp. 36-41.

Interferometry - Research and Applications in Science and Technology

Edited by Dr Ivan Padron

ISBN 978-953-51-0403-2
Hard cover, 462 pages
Publisher InTech
Published online 21, March, 2012
Published in print edition March, 2012

This book provides the most recent studies on interferometry and its applications in science and technology. It is an outline of theoretical and experimental aspects of interferometry and their applications. The book is divided in two sections. The first one is an overview of different interferometry techniques and their general applications, while the second section is devoted to more specific interferometry applications comprising from interferometry for magnetic fusion plasmas to interferometry in wireless networks. The book is an excellent reference of current interferometry applications in science and technology. It offers the opportunity to increase our knowledge about interferometry and encourage researchers in development of new applications.

InTech Europe
University Campus STeP Ri
Slavka Krautzeka 83/A
51000 Rijeka, Croatia
Phone: +385 (51) 770 447
Fax: +385 (51) 686 166
www.intechopen.com

InTech China
Unit 405, Office Block, Hotel Equatorial Shanghai
No.65, Yan An Road (West), Shanghai, 200040, China
中国上海市延安西路65号上海国际贵都大饭店办公楼405单元
Phone: +86-21-62489820
Fax: +86-21-62489821